Supercond. Sci. Technol. **23** (2010) 034004 (7pp) doi:10.1088/0953-2048/23/3/034004

Code-division multiplexing of superconducting transition-edge sensor arrays

K D Irwin[1], M D Niemack[1], J Beyer[2], H M Cho[1], W B Doriese[1], G C Hilton[1], C D Reintsema[1], D R Schmidt[1], J N Ullom[1] and L R Vale[1]

[1] National Institute of Standards and Technology, MS817.03, 325 Broadway, Boulder, CO 80305, USA
[2] Physikalisch-Technische Bundesanstalt (PTB), Abbestraße 2-12, D-10587 Berlin, Germany

Received 10 September 2009, in final form 2 December 2009
Published 22 February 2010
Online at stacks.iop.org/SUST/23/034004

Abstract
Multiplexed superconducting quantum interference device (SQUID) amplifiers have recently enabled the deployment of kilopixel arrays of superconducting transition-edge sensor (TES) detectors on a variety of receivers for astrophysics. Existing multiplexing techniques for TES arrays, however, have constraints due to aliasing of SQUID noise, the size of the required filtering elements, or the complexity of the room-temperature electronics that make it difficult to scale to much larger arrays. We have developed a Walsh code-division SQUID multiplexer that has the potential to enable the multiplexing of larger arrays or pixels with faster thermal response times. The multiplexer uses superconducting switches to modulate the polarity of coupling between N individual TES detectors and a single output SQUID channel. The polarities of the detector signals are switched in the pattern of an $N \times N$ Walsh matrix, so a frame composed of N orthogonal samples can be used to reconstruct the detector signals without degradation. We present an analysis of the circuit architecture and preliminary results.

(Some figures in this article are in colour only in the electronic version)

1. Introduction

Superconducting transition-edge sensors (TES) [1] are emerging as a leading detector for cosmic microwave background, submillimeter, and x-ray astronomy. Single TES pixels have achieved the best x-ray [2] and gamma-ray [3] energy resolution of any non-dispersive technology, and background-limited performance in the cosmic microwave background (CMB) and submillimeter. Over the last decade, the TES has developed from single-pixel demonstration devices into kilopixel cameras operating on ground-based telescopes, including the Atacama Cosmology Telescope (ACT) [4] and the South Pole Telescope (SPT) [5].

In order to develop practical kilopixel arrays, it has been necessary to develop cryogenic signal multiplexing techniques to reduce the number of wires required between temperature stages. Existing kilopixel TES arrays are read out with either time-division multiplexing (TDM) [6] or frequency-division multiplexing (FDM) [7]. While these instruments have been successful, multiplexing techniques are needed that will enable scaling to larger pixel counts and faster sensors, and that will reduce the cost and complexity of readout wiring even in smaller arrays.

In this work, we overview the cryogenic multiplexing techniques used to read out TES detectors, including TDM and FDM, which are used in fielded instruments, and code-division multiplexing (CDM), which is at an earlier stage of development. CDM shares many of the advantages of both TDM and FDM, and has the potential to significantly increase the number of pixels multiplexed in each output channel, or to enable the multiplexing of faster pixels. We present a demonstration of CDM, and describe details of the implementation of CDM and constraints on device design.

2. Cryogenic signal multiplexing

Analog signal multiplexing occurs in four basic steps: bandwidth limitation, encoding, summation, and demultiplex-

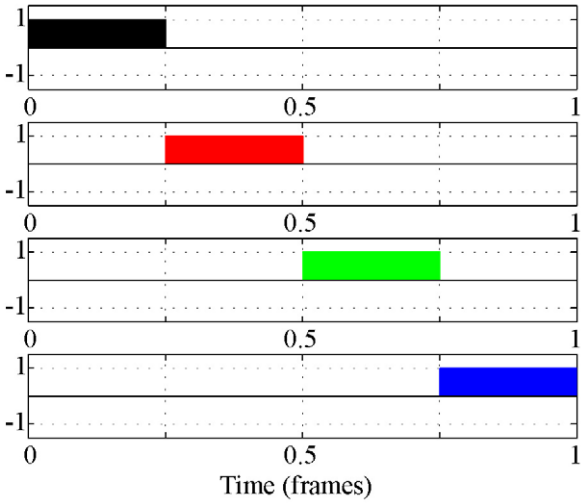

Figure 1. Time-division multiplexing modulation functions. The time (x-axis) is plotted against the output gain for the example of a four-pixel multiplexer. Orthogonal, low-duty-cycle square waves are used to turn on one channel at a time. All channels are cycled through sequentially each frame.

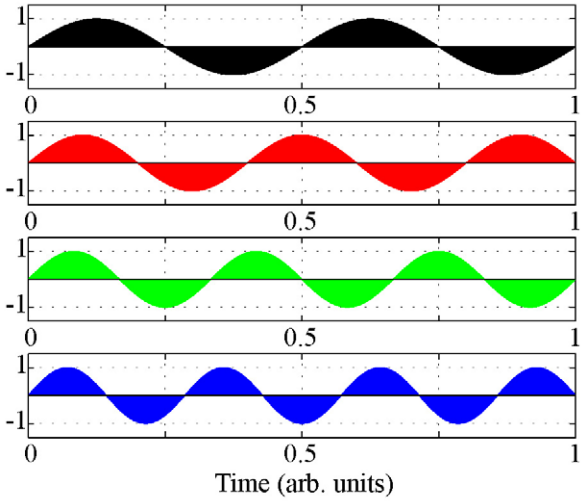

Figure 2. Frequency-division multiplexing modulation functions. The time (x-axis in arbitrary units) is plotted against the amplitude of the modulation function (arbitrary units) for the example of a four-pixel multiplexer. The output of the four different pixels is modulated at four different orthogonal frequencies.

ing/decoding. The first of these steps, bandwidth limitation, is necessary to prevent signal degradation. If the bandwidth is not limited, the out-of-band detector noise and signal power will either alias into the signal band, degrading resolution as the square root of the number of pixels multiplexed, or appear in other channels as large crosstalk.

After bandwidth limitation, the signals from different pixels are 'encoded' by multiplying them with a set of orthogonal modulation functions and summing the modulated signals into the output channel [8]. The signals can be separated and decoded at room temperature by use of the same functions. The most important sets of orthogonal modulation functions used to date to multiplex TES detectors are low-duty-cycle square wavefunctions for time-division multiplexing and sinusoidal functions for frequency-division multiplexing. We briefly review TDM and FDM, with which mature TES instruments have been deployed in the field. We then describe the Walsh modulation functions used for CDM, which has the potential to increase the scale of TES arrays that can be instrumented.

2.1. Time-division

According to the Nyquist–Shannon sampling theorem [9], if the bandwidth of a signal is limited to δf by a low-pass filter, a signal of duration δt can be exactly represented by $2\delta f \delta t$ samples in time space. If the output communication channel has a bandwidth $B \gg \delta f$, and if the amplifier noise is sufficiently low, then many input channels can be multiplexed in one output channel by sampling them sequentially. In TDM, the dissipation in a resistive thermometer such as a TES makes it possible to passively limit its bandwidth using L/R low-pass filters with relatively small inductors (typically a few hundred nanohenries for a TES with a normal resistance $R \sim 10$ mΩ).

In TDM, the signal is encoded through multiplying it by a low-duty-cycle boxcar modulation function (figure 1). If the sampling interval (the time to cycle through one frame), $\delta t_{\rm frame}$, is sufficiently short, no TES signal is aliased. However, while the bandwidth of the TES signal, δf, can be reduced to below the Nyquist sampling frequency, $1/2\delta t_{\rm frame}$, the bandwidth of the SQUID must be much larger than the Nyquist sampling frequency in order to accommodate all of the multiplexed signals. Thus, the effective noise current of the SQUID amplifier is degraded by SQUID noise aliasing. The minimum SQUID noise aliasing occurs if the bandwidth of the SQUID is itself limited by the boxcar modulating function used to encode the TESs. In frequency space, the boxcar function is a sinc function with noise bandwidth $f_{\rm n} = 1/2\delta t_{\rm line}$, where $\delta t_{\rm line} = \delta t_{\rm frame}/N$ is the line time (the period during which the multiplexer dwells on each pixel), and N is the number of pixels multiplexed in each output channel. The SQUID noise bandwidth $f_{\rm n}$ is N times larger than the Nyquist sampling frequency $f_{\rm NYQ} = 1/2\delta t_{\rm frame}$, so the SQUID noise is degraded by a factor of $\sqrt{N}$ by aliasing. This degradation factor is often referred to as the multiplex disadvantage of TDM. The SQUID must be coupled to the input channel with $\sqrt{N}$ higher mutual inductance than in the non-multiplexed case in order to avoid degradation of the input signal. This higher coupling increases the flux slew rate on the SQUID when a pulse is detected in a TES calorimeter.

2.2. Frequency-division

In FDM of a TES array, the signals in different channels are modulated by sinusoids at different frequencies (figure 2). The bandwidth is limited either by a lumped-element LCR bandpass filter for operation at megahertz frequencies [7] or by a superconducting microresonator for operation at gigahertz frequencies [10]. In the case of megahertz operation, the R is provided by the TES resistance, $R_{\rm n} \sim 1\ \Omega$, with lumped-element inductors $L \sim 10\ \mu$H and capacitors $C \sim 10$ nF. For

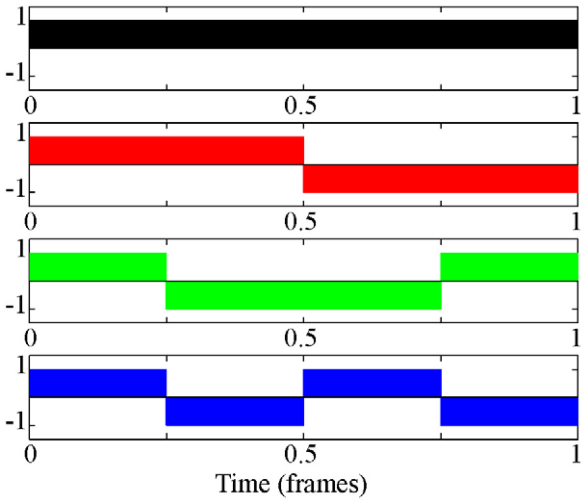

Figure 3. Code-division multiplexing modulation functions. The time (x-axis) is plotted against the output gain for the example of a four-pixel multiplexer. Orthogonal Walsh functions are used to modulate the polarity with which each pixel couples to the communications channel between positive and negative unity. A full modulation set is implemented in each frame.

gigahertz circuits, the bandpass is provided by a long ($\lambda/4$) superconducting microresonator, with bandwidth determined by the value of a coupling capacitor to a 50 Ω feedline.

For MHz circuits, the TES itself is ac biased [7]. As a highly nonlinear device, ac biasing of TES detectors can introduce operational complexities. In GHz circuits, the TES is dc biased [10], and an unshunted rf SQUID associated with the TES is ac biased at the frequency of the superconducting microresonator.

In FDM, unlike TDM, the SQUID amplifier can be limited to the same bandwidth as the TES detector, and no SQUID noise aliasing occurs. Thus, FDM does not suffer from the same multiplex disadvantage as TDM. This relaxes the requirements on the slew rate of the SQUID readout circuit. However, FDM requires much larger filter elements (larger than the filter elements and SQUID switches used in TDM), and requires more complex room-temperature readout electronics.

2.3. Code-division

A third set of orthogonal modulation functions is very promising for multiplexing TES detectors: Walsh matrices for code-division multiplexing (CDM) (figure 3). In code-division multiplexing, the signals from all TESs are summed with different polarity patterns. For instance, in the simplest case of two-channel code-division multiplexing, the sum of the signals from TES 1 and 2 would first be measured, followed by their difference. The original signals can be reconstructed from the reverse process. Depending on the implementation, CDM can use the same room-temperature electronics and firmware as TDM.

In CDM, as with TDM, the bandwidth of the SQUID must be much larger than the Nyquist frequency associated with the sampling, so the SQUID noise is degraded by a factor of $\sqrt{N}$ by aliasing. However, CDM does not suffer from the same 'multiplex disadvantage'. Because every pixel is read out at all times (but with different polarities), N independent samples of each input signal are taken each frame, which increases the signal-to-noise ratio (SNR) by $\sqrt{N}$. This increase in SNR compensates for the degradation due to SQUID noise aliasing.

CDM combines some of the best attributes of both time- and frequency-division multiplexing with SQUID amplifiers. As with time-division multiplexing, it uses simpler electronics and smaller filtering elements, and it allows dc biasing of the TES sensor. Like frequency-division multiplexing, CDM does not suffer from the 'multiplex disadvantage' of TDM from aliasing of SQUID noise. This will greatly improve the maximum slew rate and dynamic range, enabling much larger arrays.

3. Code-division multiplexing implementations

The potential advantage of code-division multiplexing of TES detectors has previously been recognized [11], but implementations that have been proposed have not been pursued because of problems with degradation of energy resolution and crosstalk. In these efforts, the Walsh matrix modulation function was implemented by changing the sign of the TES bias, which made it impossible to limit the TES bandwidth before multiplexing, leading to significant aliasing of detector noise and unavoidable degradation in TES performance.

Here we present two different approaches to code-division multiplexing that are both under active development at NIST for the readout of TES arrays. These implementations limit the bandwidth of the TES before multiplexing, so they do not suffer aliased TES noise. They promise improved array scaling and performance by eliminating the multiplex disadvantage of TDM while using its compact filter elements and simple room-temperature electronics. CDM with flux summation (section 3.1) is straightforward to develop, while CDM with current switching (section 3.2) has greater potential scalability and performance.

3.1. CDM with flux summation

A conceptually simple way to implement code-division multiplexing is to passively sum N TES signal currents in N different SQUIDs with different coupling polarities. The signals from the N SQUIDs are then measured sequentially with a conventional time-division SQUID multiplexer. In the simplest case of two-channel code-division multiplexing, the sum of the signals from TES 1 and 2 would be measured in the first SQUID, and their difference in the second. The original signals can be reconstructed from the reverse process. For large numbers of pixels, it is most convenient to sum the fluxes into superconducting transformers that couple to the SQUIDs (figure 4).

Flux-summation CDM is straightforward to implement, but it requires leads to be lithographically routed from

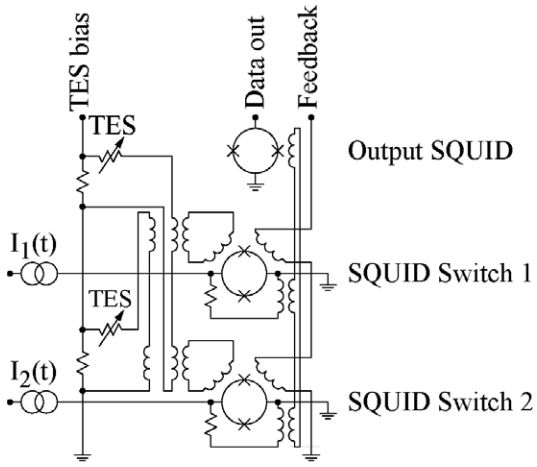

Figure 4. A two-channel implementation of code-division multiplexing by flux summation. The first SQUID switch couples to the sum of the signals from both TESs. The second SQUID switch couples to the difference of the signals from the two TESs, since the polarity of flux coupling from TES 2 to SQUID 2 is reversed, as indicated by the reversed inductor symbol. The output SQUID couples to either the sum or the difference, depending on which SQUID switch is turned on by an address current.

every TES to every SQUID, and it requires a time-division-multiplexed SQUID switch for each TES. In this approach, the orthogonal polarity code (typically a Walsh matrix) is implemented by the choice of the polarity with which the wire from each TES wraps around the different superconducting transformers. In contrast to the current-steering switch approach discussed next, the required length of lithographic leads scales as the square of the number of pixels multiplexed in each output channel. The complexity of lead routing in the flux-summation approach will provide a practical limit to how many total pixels can be multiplexed in each output channel. We are presently fabricating a 32-channel flux-summation CDM circuit that uses the same silicon chip area as our conventional TDM circuits (3 mm $\times$ 20 mm).

While flux-summation CDM lacks some of the advantages of current-steering CDM, flux-summation CDM is much simpler to implement, and may provide near-term benefits for the multiplexing of fast x-ray calorimeters for applications including the International X-ray Observatory (IXO). Since CDM does not suffer from the multiplex disadvantage, the mutual inductance of the input coil can be significantly reduced, reducing the slew rate and dynamic range requirements of the SQUID. This improvement can increase the number of pixels multiplexed, or make it possible to multiplex faster detectors.

3.1.1. Crosstalk in flux-summation CDM. Inter-pixel crosstalk is an important factor in any multiplexing circuit. Here, we consider three sources of crosstalk in flux-summation CDM: crosstalk due to inductive coupling between TES channels, crosstalk due to coupling between the feedback signal and the input circuits, and crosstalk due to aliased signal variation within one frame of CDM data.

The superconducting summing transformers in flux-summation CDM are designed to inductively couple the TESs to the SQUIDs with different polarities, but they also inductively couple the TES channels to each other. Fortunately, since the Walsh matrix is orthogonal, the inductive coupling between TES pairs cancels out across all superconducting transformers, and the net coupling is nominally zero. However, some residual coupling will remain due to imperfections in the fabrication, small variations in the summing coil inductance due to different magnetic environments, and different shielding currents in the SQUID amplifiers. The residual coupling will be a source of small inter-channel crosstalk that will need to be measured.

As in time-division SQUID multiplexing, coupling from the feedback coil to the input coil of SQUID channels that are turned off can lead to inter-pixel crosstalk. In TDM circuits, we have approximately nulled this coupling by implementing a 'dummy' SQUID adjacent to each SQUID switch, in which the inductive coupling between the feedback and input coils is equal but opposite to the coupling in the SQUID itself. The dummy SQUID, however, is not necessary in the flux-summation CDM. All TES channels (except for the first) couple with positive polarity to half of the SQUIDs, and with negative polarity to the other half. Thus, the net coupling between the feedback coil and the TES inputs is nominally zero, except for residual coupling due to fabrication imperfections, different magnetic environments, and SQUID screening. The first channel in the Walsh code, however, always has positive polarity, and thus will have larger crosstalk from the feedback signals of the other channels. It may be advisable not to use the first channel, in which case a 32-channel CDM circuit would practically read out 31 TES detectors.

Finally, in both flux-summation CDM and current-steering CDM, if the signal coming from any pixel changes significantly during a frame time, the result will be a crosstalk signal in the 'nearest neighbor' pixels in Walsh space. This effect is analogous to power leaking from a pixel at one frequency in FDM to a pixel at a nearest neighbor frequency. As in FDM, crosstalk is mitigated by bandwidth limiting the pixel. In CDM, this bandwidth limitation is provided by the L/R low-pass filter before the signal is modulated by the Walsh code, while in FDM the bandwidth is limited by an LCR bandpass filter. However, without a true sample-and-hold circuit that keeps all signals constant during a frame, there will be residual crosstalk. A software correction is possible for the portion of residual crosstalk that is caused by linear signal variations within a frame. The implementation of linear drift correction in software reduces crosstalk to a negligible level in Monte Carlo models of high resolution multiplexed TES x-ray calorimeters.

3.2. CDM with current steering

A more ambitious implementation of CDM uses a single-pole double-throw (SPDT) superconducting switch (after the signal bandwidth is limited by an inductive filter) to modulate the polarity with which the TES couples to the SQUID amplifier

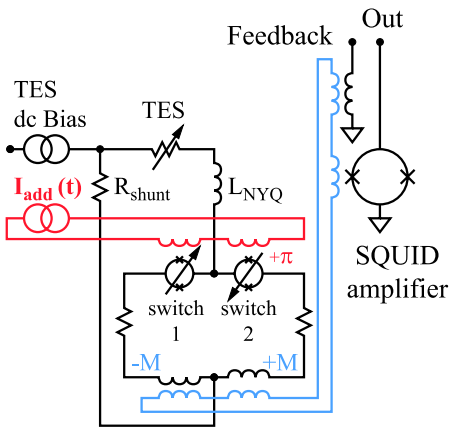

Figure 5. A single-pole double-throw polarity switch. Two superconducting-to-normal SQUID switches (switch 1 and switch 2) steer the current from the TES into two different arms of the circuit. One arm couples to the SQUID amplifier with positive polarity (mutual inductance $+M$) and the other with negative (mutual inductance $-M$). Switch 2 is offset by π phase from the other by an externally applied flux (offset flux line not shown). The address current $I_{\rm add}(t)$ applies flux to change which SQUID is superconducting. In a multiplexer, many TES detectors are coupled through polarity switches to a single SQUID.

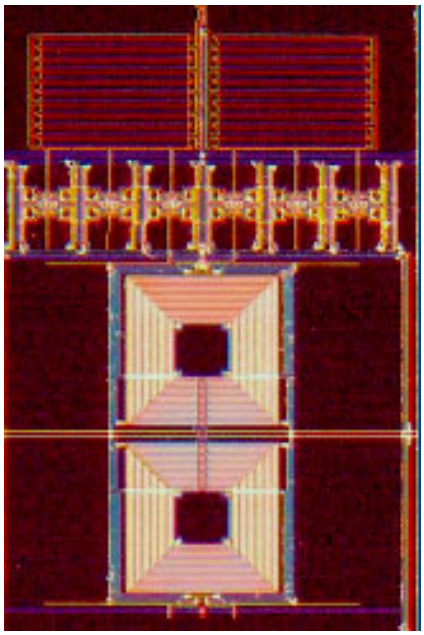

Figure 6. A photograph of a single-pole double-throw polarity switch that is part of a four-channel CDM circuit. The series resistors in the two arms of the SPDT switch are on the top, the flux-actuated superconducting-to-normal switches are in the middle, and a summing inductor wound as a gradiometer is on the bottom. Four channels of these switches have their output summed into a single SQUID amplifier channel.

(figure 5). The polarity modulation occurs at much higher frequency than the bandwidth-limited signal, so there is no degradation in performance from detector noise aliasing.

The two circuit arms of the SPDT superconducting switches contain superconducting-to-normal switches based on a low inductance dc SQUID [12]. The superconducting-to-normal switch is a SQUID configured to operate as a variable resistor controlled by an applied flux. The critical current of a dc SQUID modulates from a value of $I_{\rm c} = 2I_0$ at zero flux to a minimum value at flux $\Phi = \Phi_0/2$, where I_0 is the critical current of a single junction. It can be shown by Taylor expansion in the limit of low $\beta_{\rm L} \equiv 2LI_0/\Phi_0$ (where L is the SQUID loop inductance) that the critical current of a dc SQUID approaches $I_{\rm c} = \pi I_0^2 L/\Phi_0$ for $\Phi = \Phi_0/2$. If this value is low enough, the dc SQUID will be normal for all signals of interest.

The two arms of the SPDT circuit are actuated by a flux from an applied address current $I_{\rm add}(t)$, but the second arm has an additional π phase offset provided by $\Phi_0/2$ flux from a π phase line common to the entire array. When no flux is applied by the address line, switch 2 is 'off' (in the low critical current state), and switch 1 is 'on' (in the high critical current state), and almost all of the TES current flows through switch 1. As the address flux is changed by $\Phi_0/2$, switch 1 is driven into the resistive state, and switch 2 becomes superconducting, which causes the signal to flow through switch 2.

The polarity modulation can be achieved either by the current-steering topology shown in figure 5, or a transformer-coupled current switch. In the transformer-coupled current switch, the current from each TES inductively couples to two different superconducting transformers that couple to the output SQUID with opposite polarity. Superconducting-to-normal switches are in each loop. When driven normal, these switches prevent flux coupling in that transformer arm. They can be driven normal by applying a bias current to the transformer loop or by applying an address flux. While both the transformer-coupled current switch and the current-steering switch are under development, in this paper we focus principally on the current-steering switch of figure 5.

3.2.1. Demonstration of current-steering CDM. We have demonstrated a four-channel CDM multiplexer using current-steering SPDT switches based on the schematic in figure 5. A photo of a single SPDT switch is shown in figure 6. It is a gradiometric design that is relatively insensitive to stray magnetic fields. Four different signals (square wave, triangle wave, sine wave and sawtooth) were inject by signal generators into the four channels. The output of the SQUID was read out using standard TDM room-temperature electronics, which addressed the lines in the pattern of the 4×4 Walsh matrix, provided switched digital feedback to linearize the SQUID, and took a data sample each line time $\delta t_{\rm line} \equiv \delta t_{\rm frame}/N$ after allowing the switching transients to settle.

The result was the multiplexed data stream shown in figure 7. The data stream was demultiplexed using the inverse Walsh matrices. The demultiplexed data are shown in figure 8. The demultiplexing recovered the input signals with high fidelity. The polarity of the coupling of the pixels to the SQUID is modulated in all TES channels except the one channel corresponding to the first column of the Walsh matrix. This modulation has the effect of removing low frequency noise in the SQUID as well as any pickup in the SQUID amplifier chain at frequencies below the frame rate. In figure 8, the

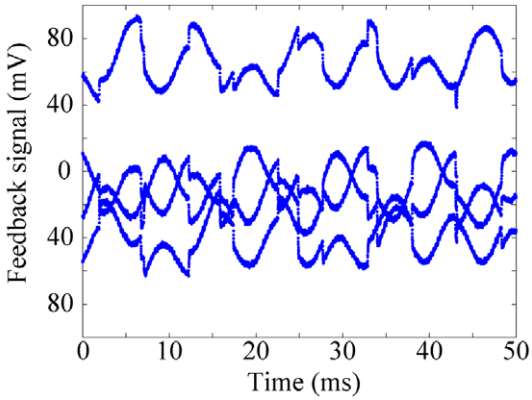

Figure 7. A multiplexed data set taken with a four-pixel CDM circuit. The data set consists of rapid switching between four Walsh polarity combinations of four input signals.

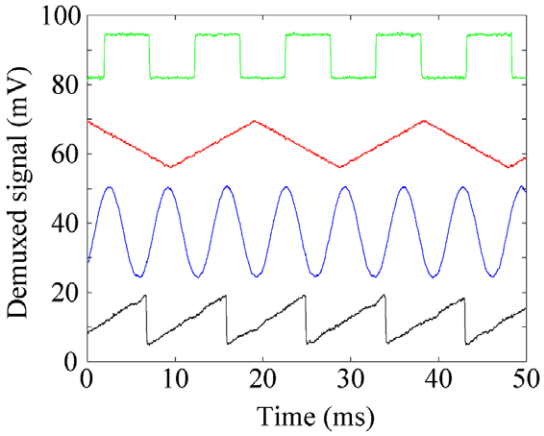

Figure 8. The data set in figure 7 demultiplexed by multiplying it by the inverse Walsh matrix. The input signals (a square wave, triangle wave, sine wave, and sawtooth) are recovered with high fidelity. Differencing removes low frequency noise and pickup in all channels except for the sawtooth.

non-modulated pixel corresponds to the sawtooth input signal. While the noise in all three other pixels appears white, there is additional structure in the demultiplexed sawtooth signal that evidences non-white noise. Thus, if the first Walsh column is not used to read out a TES, low frequency and pickup noise in the amplifier is removed by multiplexing.

3.2.2. Current-steering back action. One constraint on circuits using the current-steering circuit topology is the voltage generated by a switch of the current pathway, which has a back action effect on the TES. Within the bandwidth of the TES filter, this back action has a particularly simple form: it appears as an additional switch load resistance in series with the TES. During a switching event, the time integral of the voltage generated is equal to the flux through the inductor coupled to the SQUID:

$$\int V \, \mathrm{d}t = \Phi = I L_{\mathrm{sw}}, \tag{1}$$

which is proportional to L_{sw}, the self-inductance of the inductor coupling the switch to the SQUID, and the TES current I. The average voltage is

$$V_{\mathrm{avg}} = \int V \, \mathrm{d}t / \tau_{\mathrm{dwell}}, \tag{2}$$

the integral voltage during a switching event divided by τ_{dwell}, the average period between switching events. Thus, within the bandwidth of the low-pass filter, the voltage appears as a dc voltage proportional to the current, with an effective switch resistance

$$R_{\mathrm{sw}} = L_{\mathrm{sw}} / \tau_{\mathrm{dwell}}. \tag{3}$$

The value of R_{sw} must be kept small as compared to the TES bias resistance in order to maintain a voltage bias. If a voltage bias is maintained, the power dissipated during switching events will also be small as compared to the bias power of the TES.

3.2.3. Josephson oscillations. Another constraint in the current-steering switches is caused by Josephson frequency oscillations. The voltage applied to the switch that is off will cause it to oscillate at frequency V/Φ_0. In the current-steering circuit, this voltage is determined by the product of the TES bias current and the series resistance in the switch, which must be small as compared to the TES resistance. The switch must be designed to keep this frequency sufficiently far out of the signal band.

3.2.4. Sub-frame sampling. One important limiting factor in time-division multiplexing of fast TES x-ray calorimeters is caused by systematic variation in the measured photon energy as a function of the time at which the x-ray photon arrived within a frame of sampled data. This variation can be partially compensated in software, but often the required sampling rate is determined principally by variations in photon arrival time within a frame. In TDM, the output of each pixel is measured only once each frame time, but in CDM the output of each pixel is measured once each line time (N times more frequently). Both flux-summing and current-steering CDM circuits have the potential advantage over TDM of this sub-frame sampling. Since the signals from all TESs are measured in every row (but with different polarity) rather than just once each frame, information about the photon arrival is available on timescales small compared to the frame time. One way to make use of this information is to determine the definition of a frame dynamically to align it with the row in which the x-ray photon initially arrives. The resulting matrix, if shifted by several rows from the conventional start row, is not identical to the Walsh matrix, but it is still orthogonal and invertible, so multiplexing can occur in the same way. The systematic variation in photon arrival time is thus reduced from the frame time to the row time, which has the potential to significantly improve TES calorimeter array performance.

3.2.5. Binary addressing. CDM implementations based on flux-actuated switches, including current-steering devices, also have the potential advantage of greatly reducing the number

of address line wires. With flux-actuated CDM, it is possible to address N rows of TES pixels using many fewer than N address lines. Binary encoding of the address lines is made possible by the periodic nature of the response of the superconducting interferometer switches to address flux. If one address line applies $\Phi_0/2$ addressing flux, switching a row of pixels to a negative gain, an additional $\Phi_0/2$ flux provided by a second address line will switch the gain back to positive. By selecting which address lines couple to which rows, it is possible to implement a full Walsh matrix modulation function for N rows with $\log_2 N$ address lines. As a simple example, consider multiplexing of four pixels with CDM, numbered from 0 to 3. If the first address line is coupled to pixels 2 and 3, and a second address line is coupled to pixels 1 and 2, then all four Walsh codes can be accessed by changing the flux through the two lines. Then address fluxes of $0, 0$ leaves all gains positive, (1 1 1 1), address flux $\Phi_0/2, 0$ gives (1 1 -1 -1), address flux $0, \Phi_0/2$ gives (1 -1 -1 1), and address flux $\Phi_0/2, \Phi_0/2$ gives (1 -1 1 -1): a full Walsh code modulation set. In principle, 256 rows of TES detectors could be addressed with only eight address lines.

4. Conclusions

The code-division SQUID multiplexer uses the same simple room-temperature electronics and compact cryogenic filter elements as TDM, but it does not suffer from the multiplex disadvantage caused by aliased SQUID noise. The simple flux-summation CDM implementation has the potential to increase the speed of fast TES x-ray microcalorimeter arrays for applications including the International X-ray Observatory. This advantage arises from a reduction of the required flux slew rate in the SQUID, and the potential for sub-frame sampling. The speed of the x-ray calorimeters in a CDM array could potentially be increased over that of a TDM array by a factor as large as $N^{1/3}$, where N is the multiplexing factor. The magnitude of this advantage depends on the details of the specific implementation, because the frame sample rate must still be higher than the Nyquist frequency of the highest detector signal of interest, and the required flux slew rate depends on whether the x-ray source is a point source, or is uniformly distributed across the array.

The more advanced current-steering architecture may provide additional increase in the scalability of TES x-ray calorimeters and long-wavelength bolometers, but careful design is required to avoid problems caused by switch back action and Josephson oscillations. In addition to sub-frame sampling and a reduction in flux slew rate, current-steering CDM has the advantage of binary addressing and ultra-low power dissipation in the focal plane.

Acknowledgment

This work was supported in part by NASA under contract NNG09WF27I.

References

[1] Irwin K D 1995 *Appl. Phys. Lett.* **66** 1998–2000
[2] Kilbourne C A *et al* 2008 *J. Low Temp. Phys.* **151** 223–8
[3] Doriese W B 2007 *Appl. Phys. Lett.* **90** 193508
[4] Hincks A D 2009 *Astrophys. J.* submitted (arXiv:0907.0461)
[5] Carlstrom J *et al* 2009 *PASP* submitted (arXiv:0907.4445)
[6] Chervenak J A, Irwin K D, Grossman E N, Martinis J M, Reintsema C D and Huber M E 1999 *Appl. Phys. Lett.* **74** 4043–5
[7] Yoon J, Clarke J, Gildemeister J M, Lee A T, Myers M J, Richards P L and Skidmore J T 2001 *Appl. Phys. Lett.* **78** 371–3
[8] Kiviranta M, Seppä H, van der Kuur J and de Korte P 2002 *AIP Conf. Proc.* **605** 295–300
[9] Shannon C E 1949 *Proc. Inst. Radio Eng.* **37** 10–21
[10] Mates J A B, Hilton G C, Irwin K D, Vale L R and Lehnert K W 2008 *Appl. Phys. Lett.* **92** 023514
[11] Karasik B S and McGrath W R 2001 *Proc. 12th Int. Symp. on Space Terahertz Technology (San Diego, CA, Feb.)* pp 436–45
Podt M, Weenink J, Flokstra J and Rogalla H 2002 Coded SQUID arrays *Physica* C **368** 218–21
[12] Beyer J and Drung D 2008 *Supercond. Sci. Technol.* **21** 105022